

Are General-Purpose Vision Models All We Need for 2D Medical Image Segmentation? A Cross-Dataset Empirical Study

Vanessa Borst¹[0009-0004-7123-7934] 
and Samuel Kounev¹[0000-0001-9742-2063]

Julius-Maximilians-University Würzburg, 97070 Würzburg, Germany
{vanessa.borst,samuel.kounev}@uni-wuerzburg.de

Abstract. Medical image segmentation (MIS) is a fundamental component of computer-assisted diagnosis and clinical decision support systems. Over the past decade, numerous architectures specifically tailored to medical imaging have emerged to address domain-specific challenges such as low contrast, small anatomical structures, and limited annotated data. In parallel, rapid progress in computer vision has produced highly capable general-purpose vision models (GP-VMs) originally designed for natural images. Despite their strong performance on standard vision benchmarks, their effectiveness for MIS remains insufficiently understood. In this work, we conduct a controlled empirical study to examine whether specialized medical segmentation architectures (SMAs) provide systematic advantages over modern GP-VMs for 2D MIS. We compare eleven SMAs and GP-VMs using a unified training and evaluation protocol. Experiments are performed across three heterogeneous datasets covering different imaging modalities, class structures, and data characteristics. Beyond segmentation accuracy, we analyze qualitative Grad-CAM visualizations to investigate explainability (XAI) behavior. Our results demonstrate that, for the analyzed datasets, GP-VMs outperform the majority of specialized MIS models. Moreover, XAI analyses indicate that GP-VMs can capture clinically relevant structures without explicit domain-specific architectural design. These findings suggest that GP-VMs can represent a viable alternative to domain-specific methods, highlighting the importance of informed model selection for end-to-end MIS systems. All code and resources are available at GitHub.

Keywords: Medical image segmentation · Empirical Evaluation · Deep learning · General-purpose vision models

1 Introduction

Accurate segmentation of medical images plays a central role in computer-assisted diagnosis, treatment planning, and longitudinal disease monitoring. The emergence of deep learning has fundamentally transformed this field, enabling increasingly precise delineation of anatomical structures and pathological regions across imaging modalities. Since the introduction of the seminal U-Net

architecture [18], the medical imaging community has produced a variety of domain-specific architectures [21]. These approaches aim to address challenges inherent to medical data, including the detection of small target structures, limited availability of annotated datasets, severe class imbalance, and robustness under challenging clinical conditions characterized by variable image quality and domain-specific artifacts. Many proposed methods build upon the U-Net paradigm while incorporating advances from modern deep learning research, including transformer-based mechanisms [9], multi-scale feature modeling [8], state-space layers for long-range dependency modeling [14], and alternative architectural paradigms such as Kolmogorov–Arnold Networks (KANs) [13].

In parallel, the broader computer vision community has witnessed rapid progress in powerful GP-VMs designed for dense prediction tasks, such as semantic segmentation (SS) and object detection. Modern backbones [20,24] leverage large-scale pretraining on natural image corpora followed by lightweight fine-tuning for downstream tasks. Such models, potentially combined with advanced decoders [27], demonstrate strong performance on challenging benchmarks such as ADE20K [29], usually exhibiting robust generalization. Notably, GP-VMs often benefit from extensive optimization, comprehensive ablation studies, and validation on millions of images—resources that are rarely available for MIS.

This progress raises a fundamental question for MIS: Do medical segmentation tasks truly require specialized medical segmentation architectures, or can general-purpose vision models achieve comparable performance? Initial studies have begun exploring transfer learning and cross-domain adaptation in medical imaging. For example, the Segment Anything Model (SAM) [11], a milestone in general-purpose (GP) SS, has already been adapted to medical contexts [28,1]. Other works have demonstrated that large-scale ImageNet-pretraining can yield robust feature representations for medical analysis [14]. Recent research in wound segmentation has reported that GP-VMs can outperform medical approaches and even challenge-winning wound-targeted methods [2]. Concurrently, recent survey papers have begun to explore the broader role of generalist models in healthcare. Some studies focus specifically on SAM and its successors [1], whereas others examine generalist approaches in healthcare more broadly [10]. Notably, a 2026 review systematically evaluated generalist models for MIS, benchmarking them against task-specific architectures across multiple anatomical targets, and reported that generalist models frequently achieve top-tier performance [16].

Despite these encouraging findings, certain limitations remain. Survey studies typically rely on metrics reported in original publications [16], which must be interpreted cautiously due to the absence of standardized evaluation protocols. In practice, studies often differ substantially in datasets, pre-processing pipelines, augmentation strategies, optimization settings, and evaluation procedures, all of which can strongly influence reported performance [17,23]. Consequently, performance gains attributed to architectural innovations may instead arise from experimental design choices rather than intrinsic model superiority.

We address the lack of controlled empirical studies by taking an initial step toward a systematic cross-dataset comparison. Our contributions are threefold:

1. Comprehensive Empirical Study. We conduct a cross-dataset evaluation using three heterogeneous MIS datasets: (i) RGB binary lesion segmentation, (ii) RGB multi-class polyp segmentation, and (iii) grayscale multi-class cardiac region segmentation. Across these datasets, we benchmark eleven architectures, including transformer-based, state-space, KAN-based, and U-Net-style SMAs as well as recent GP SS and vision models.

2. Standardized Benchmarking Framework We establish a rigorous evaluation protocol that controls confounding factors, including dataset-specific augmentation and consistent training procedures. Beyond segmentation accuracy, we provide XAI attribution maps, enabling a more holistic comparison.

3. Practical Insights. We show that GP-VMs can serve as viable alternatives to SMAs, achieving superior performance to domain-specific models in our experiments under standardized conditions. These findings underscore the importance of informed and resource-conscious model selection in MIS research.

2 Benchmarking Methodology

2.1 Model Selection

Given the rapid growth of (medical) SS models and GP-VMs, including all recent methods is impractical. We therefore organize the comparison into two principal model families, aiming to construct a balanced and representative evaluation:

1. SMA: We include four models that are specifically designed for MIS: HiFormer-B [8], MISSFormer [9], U-KAN-L [13], and Swin-UMamba [14]. These models represent diverse modern design paradigms, including pure transformers, hybrid CNN-transformer designs, KAN integration, and state-space modeling via Mamba [6] blocks. Lastly, U-Net [18] is included as a baseline.

2. GP-VM: To assess cross-domain transferability, we include GP-VMs originally developed for natural-image understanding. This category comprises (i) SS architectures and (ii) modern vision backbones (VB) adapted for SS using a UPerHead [25] decoder. The former include SegFormer-B3 [26], SegNeXt-L [7], and VWFormer [27] with two different backbones, MiT-B3 and ConvNeXt-S. The latter are represented by InternImage-T [24] and TransNeXt-Tiny [20].

The final selection (cf. Table 1) was mainly informed by four criteria: (I) architectural diversity across CNN-, ViT, hybrid-, and emerging paradigms, (II) comparable computational scale where feasible, (III) scientific visibility in peer-reviewed venues, and (IV) public code availability to reduce reproduction bias.

2.2 Dataset Selection

We evaluate all models on three heterogeneous MIS datasets: ISIC’18 [4,22], BKAI-IGH NeoPolyp Small [19], and CAMUS [12]. As summarized in Table 2, the datasets differ in imaging modality, class configuration (binary vs. multi-class), and task characteristics, enabling the assessment of cross-domain performance under controlled conditions. Pre-processing and data augmentation are

Table 1: Overview of the selected methods.

Category	Architecture	Type	Size	Venue	Year
SMA	U-Net [18]	CNN	31M	MICCAI	'15
	HiFormer-B [8]	Hybrid (CNN-ViT)	26M	WACV	'23
	MISSFormer [9]	Transformer	42M	IEEE TMI	'23
	Swin-UMamba [14]	Hybrid (State-space)	60M	MICCAI	'24
	U-KAN-L [13]	Hybrid (CNN+KAN)	25M	AAAI	'25
GP-VM (SS)	SegFormer-B3 [26]	Transformer	47M	NeurIPS	'21
	SegNeXt-L [7]	CNN	49M	NeurIPS	'22
	2× VWFormer [27]	-Depends ¹		ICLR	'24
GP-VM (VB)	InternImage-T [24] ²	CNN	58M	CVPR	'23
	TransNeXt-Tiny [20] ²	Transformer	58M	CVPR	'24

¹ 51M with MiT-B3 (VW-MiT)/ 57M with ConvNext-S (VW-Conv)² Parameter count includes UPerHead decoderTable 2: Dataset overview (N : images after filtering, C : classes).

Dataset	Modality	Color	N	C	Targets	Characteristic
ISIC'18	Dermoscopy	RGB	3 565	2	Lesions	Irregular boundaries
NeoPolyp	Endoscopy	RGB	945	3	Polyps	Subtype variability
CAMUS	Echocardiography	Gray	1 996	4	Cardiac regions	Noisy ultrasound data

adapted to each modality but applied identically across architectures. To prevent potential data leakage, we perform dataset-specific filtering procedures that remove duplicate and highly similar images based on identical raw bytes and perceptual hash similarity. Details about data augmentation and image filtering are provided on GitHub. For evaluation, we employ five-fold cross-validation (CV) with uniformly sized folds. Random image-level splits are used for NeoPolyp and ISIC'18, while patient-aware splitting is applied to CAMUS, where patient identifiers are available, in order to avoid subject-level information leakage.

2.3 Standardized Training and Evaluation Protocol

Training. For fair benchmarking, all models are trained under a unified protocol while preserving architecture-specific design choices recommended by the original authors or official implementations. Standardized settings include ImageNet-pretrained encoders, an input resolution of 512×512 , AdamW optimization with Reflected Exponential (REX) learning-rate scheduler [3], batch size 8, and dataset-specific loss functions (binary cross-entropy for ISIC'18, cross-entropy for multi-class training). Within each dataset, augmentation pipelines are identical across all methods. As learning-rate sensitivity differs across architectures, a pre-defined search over $\{10^{-4}, 5 \times 10^{-5}, 10^{-5}\}$ is performed for each model–dataset pair, training each configuration for 100 epochs. The best setting based on validation mean Intersection over Union (mIoU) is used for five-fold CV with a training budget of 150 epochs and identical early stopping criteria across runs.

Evaluation. Segmentation performance is measured using mIoU, Dice Similarity Coefficient (mDSC), recall (mRec), and precision (mPrec), each computed

without background class using global micro-averaging. Model interpretability is analyzed using Grad-CAM visualizations for selected test samples. Heatmaps are generated with a modified M3d-CAM implementation [5] using `layer='auto'`, which automatically selects the last suitable layer for extracting attention maps.

Implementation. All models are trained using PyTorch 2.5.1 (Python 3.11) on two NVIDIA A100 GPUs with mixed-precision training [15], except for SegNeXt due to instability. Deterministic execution is enabled wherever supported. Deviations from the unified setup include the following: MISSFormer and HiFormer, which internally operate at 224×224 resolution; U-KAN, which lacks ImageNet-pretrained checkpoints and is therefore trained from scratch; and VWFormer, for which we solved incomplete configuration details by setting `nheads=1` and enabling shortcuts. All source code and details are available at GitHub.

3 Evaluation

3.1 Segmentation Performance

Table 3 reports the 5-fold CV results, using mDSC as main performance metric.

GPV models outperform medical architectures. Measured by the average mDSC across all three datasets, the top-performing models are exclusively GP-VMs: VW-MiT (91.0%), VW-Conv and TransNeXt (both 90.9%), followed by InternImage (90.8%) as well as SegNeXt and SegFormer (both 90.7%). In contrast, the best-performing SMA, SU-Mamba, achieves an average mDSC of 90.5%, indicating broadly comparable performance. It is followed by HiFormer with 88.8%, while the remaining SMAs achieve substantially lower average mDSC scores (≤ 87.9), trailing GP-VMs by several percentage points.

SwinUMamba is the strongest included SMA. Within the SMA family, SU-Mamba consistently achieves the best performance across all three datasets in terms of both mDSC and mIoU. Its results remain close to those of the best-performing GP-VMs, with only marginal differences. Notably, on the NeoPolyp dataset, the remaining SMAs fall considerably behind SU-Mamba, with performance gaps of more than 4 percentage points.

Performance differences are dataset-dependent. Performance disparities are largest on NeoPolyp and smaller on the other datasets. Class-wise mDSC analysis indicates increased dataset difficulty, as all models struggle to reliably segment class C_1 (non-neoplastic polyps). Here, the performance gap between GP-VMs and SU-Mamba is substantial (up to 7 percentage points), while SU-Mamba itself maintains a clear margin over the remaining SMAs. For CAMUS, class-wise metric differences are less pronounced and model performance is more similar overall; however, the left ventricular wall (LV Wall; C_2) appears slightly more challenging to segment than the left ventricle (LV) and left atrium (LA).

Summary. GP-VMs show their largest advantage on NeoPolyp, where both VWFormer variants and InternImage achieve 88.7–89.6% mDSC compared to 82.5–84.6% for most SMAs. This gap decreases on ISIC'18 and CAMUS (≈ 1 –2%); however, GP-VMs generally remain superior across modalities, with SU-Mamba and, in some cases, HiFormer being the only SMAs performing comparably.

Table 3: Per-dataset metrics (mean±SD, %; best per family in bold).

Model	mDSC	mIoU	mRec	mPrec	Class-wise mDSC ¹			
					C_1	C_2	C_3	
NeoPolyp	U-Net	83.3±1.1	71.3±1.6	80.8±3.6	86.1±2.4	34.9±18.2	88.1±0.6	–
	HiFormer	84.6±0.9	73.4±1.3	82.6±1.0	86.8±1.9	52.7±4.9	88.9±0.7	–
	MISSFormer	82.9±1.6	70.9±2.4	80.9±1.8	85.1±2.4	42.0±6.5	87.5±1.8	–
	SU-Mamba	88.9±0.6	80.0±1.0	87.3±1.3	90.6±0.9	59.2±3.8	92.5±0.6	–
	U-KAN	82.5±1.7	70.3±2.5	79.2±2.0	86.1±2.1	36.9±12.2	87.1±0.9	–
	SegFormer	89.1±1.3	80.4±2.0	87.5±2.3	90.9±1.0	63.8±4.9	92.7±0.5	–
	SegNeXt	89.2±0.7	80.5±1.2	87.8±1.8	90.7±1.4	63.6±4.2	92.8±0.8	–
	VW-Conv	89.6±1.3	81.2±2.1	88.9±2.5	90.4±1.2	63.5±6.1	93.0±0.7	–
	VW-MiT	89.7±0.8	81.3±1.4	88.5±2.0	90.9±1.8	66.1±4.3	92.7±0.9	–
	InternImage	89.6±1.1	81.2±1.7	88.2±2.0	91.1±1.1	66.0±5.7	92.9±0.7	–
TransNeXt	89.4±0.7	80.9±1.1	88.5±2.4	90.5±1.9	62.4±2.9	92.8±0.6	–	
CAMUS	U-Net	89.1±0.3	80.4±0.5	88.5±0.2	89.8±0.5	93.3±0.3	85.6±0.2	88.6±0.7
	HiFormer	90.8±0.2	83.2±0.3	91.1±0.2	90.6±0.4	94.2±0.2	87.7±0.2	91.1±0.2
	MISSFormer	90.4±0.1	82.5±0.2	90.3±0.3	90.5±0.2	93.8±0.1	87.2±0.2	90.7±0.2
	SU-Mamba	91.3±0.3	83.9±0.5	91.1±0.4	91.4±0.3	94.4±0.3	88.3±0.3	91.4±0.4
	U-KAN	90.5±0.2	82.7±0.3	90.6±0.1	90.5±0.4	94.0±0.2	87.4±0.2	90.6±0.4
	SegFormer	91.5±0.1	84.4±0.1	91.5±0.2	91.6±0.2	94.6±0.1	88.7±0.1	91.8±0.3
	SegNeXt	91.6±0.1	84.6±0.2	91.6±0.2	91.7±0.2	94.7±0.2	88.8±0.1	91.8±0.3
	VW-Conv	91.4±0.1	84.2±0.2	91.6±0.4	91.3±0.2	94.5±0.2	88.6±0.2	91.6±0.1
	VW-MiT	91.6±0.1	84.5±0.2	91.4±0.2	91.7±0.1	94.6±0.2	88.7±0.2	91.8±0.2
	InternImage	91.4±0.2	84.1±0.4	91.7±0.2	91.0±0.5	94.5±0.2	88.5±0.2	91.5±0.4
TransNeXt	91.5±0.1	84.3±0.2	91.7±0.3	91.3±0.4	94.6±0.1	88.7±0.1	91.6±0.3	
ISIC'18	U-Net	89.0±0.9	80.1±1.5	86.7±1.8	91.4±0.4	–	–	–
	HiFormer	91.0±0.6	83.4±0.9	89.2±1.2	92.8±1.0	–	–	–
	MISSFormer	90.3±0.8	82.3±1.3	88.2±1.6	92.5±0.5	–	–	–
	SU-Mamba	91.3±0.5	84.1±0.9	88.7±1.0	94.2±0.5	–	–	–
	U-KAN	89.2±1.1	80.6±1.7	86.8±1.8	91.9±1.4	–	–	–
	SegFormer	91.3±0.8	83.9±1.3	89.1±1.0	93.5±1.1	–	–	–
	SegNeXt	91.4±0.6	84.1±1.0	89.6±1.9	93.3±1.0	–	–	–
	VW-Conv	91.5±0.4	84.3±0.7	89.5±0.8	93.6±1.0	–	–	–
	VW-MiT	91.7±0.5	84.6±0.9	90.1±1.0	93.3±0.9	–	–	–
	InternImage	91.3±0.4	84.0±0.7	89.6±0.9	93.0±0.5	–	–	–
TransNeXt	91.9±0.7	85.0±1.3	90.2±1.3	93.7±0.3	–	–	–	

¹ NeoPolyp: C_1 - non-neoplastic; C_2 - neoplastic | CAMUS: : C_1 - LV; C_2 - LV Wall; C_3 - LA

3.2 Explainability Insights

Figure 1 shows the ground truth (GT), model predictions, and corresponding XAI maps for each class, using examples among the 50 worst-performing cases per fold that were challenging across all architectures. The visualization suggests that models with lower performance in Table 3 (e.g., MISSFormer) also encounter greater difficulties on these cases. Notably, the GP-VMs models consistently focus on clinically relevant regions, in some cases more precisely than certain SMAs models, as exemplified by the ISIC'18 case. Detection of non-neoplastic polyps (C_1) remains challenging for all methods, with HiFormer and U-KAN showing no attention to this class at all. In the CAMUS example, the left atrium (C_3) appears to be particularly difficult. Here, SMAs models—including the best-performing SU-Mamba—detect fewer true positives than most of the GP-VMs, which is also reflected in their stronger attention maps for C_3 in this region.

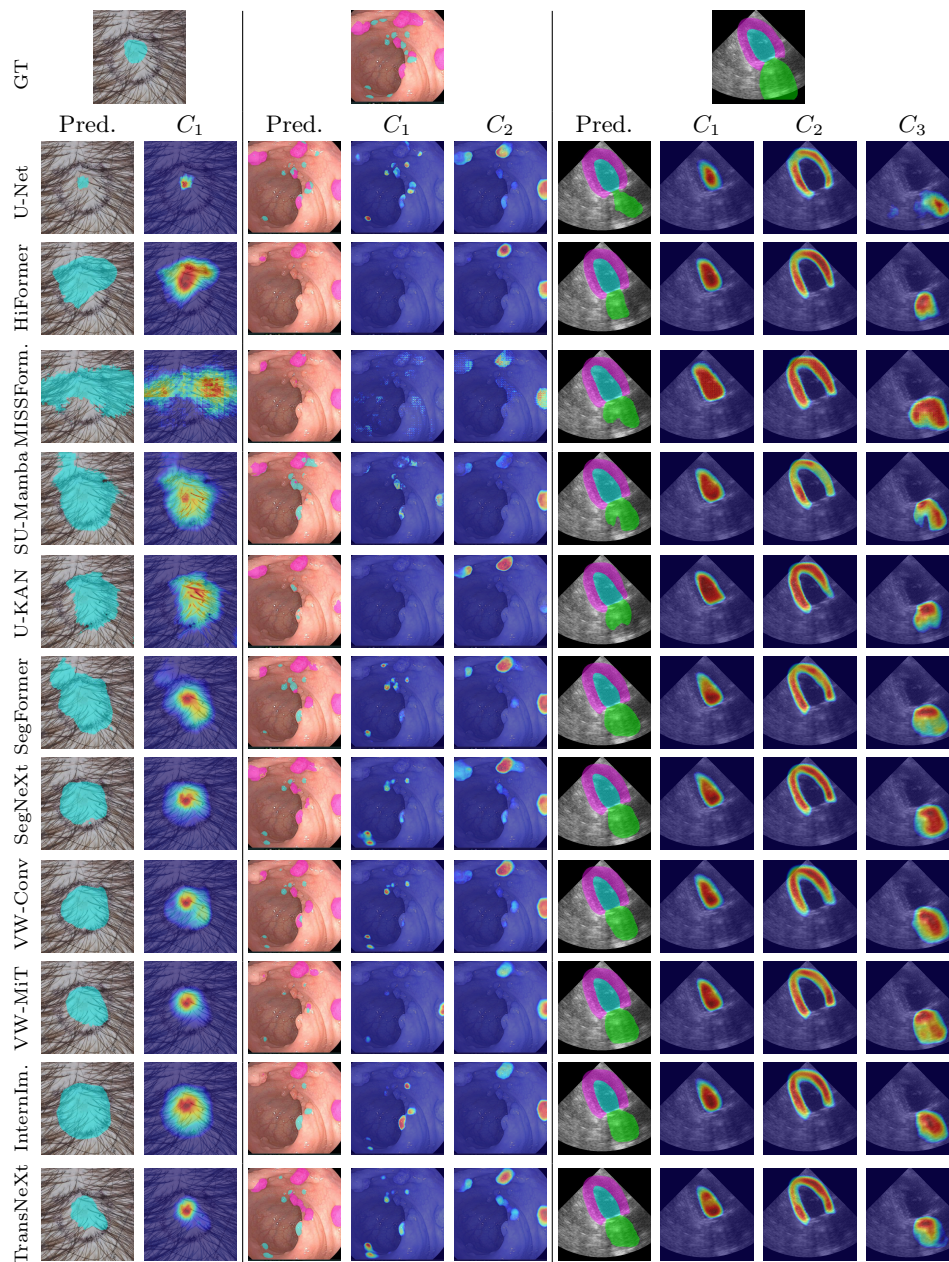


Fig. 1: Grad-CAM comparison across datasets and architectures.

4 Discussion and Conclusion

This study presents a controlled, empirical comparison of SMAs and modern GP-VMs across three heterogeneous clinical imaging tasks. Our results suggest that GP-VMs achieve segmentation performance comparable to, and in our experiments surpassing, the majority of evaluated SMAs, while producing clinically plausible attention maps. However, these findings do not imply that domain-specific architectures lack value. Medical dataset characteristics, annotation quality, and clinical objectives vary widely, and specialized models may still be advantageous for certain tasks, data regimes, or deployment scenarios. Rather, our results highlight that GP-VMs can serve as a viable alternative, emphasizing the importance of informed model selection. From a practical perspective, these findings have important implications for resource allocation. Leveraging existing GP-VMs can substantially reduce the computational and labor costs associated with developing novel architectures, freeing resources for rigorous data curation, optimized training protocols, and systematic evaluation of out-of-distribution (OOD) generalization—activities that may yield greater impact in real-world clinical settings than incremental architectural innovation alone.

Threats to validity. Our findings are limited to the considered datasets, imaging modalities, and training protocol, and may not generalize to other 2D MIS tasks, 3D imaging settings, or extremely low-data regimes. Although the selected datasets cover heterogeneous characteristics, they cannot fully represent the diversity of clinical imaging, and alternative benchmark designs may lead to different outcomes. Moreover, although a representative model set was selected, the comparison is inherently limited by the chosen architectures. Models with fewer parameters such as U-KAN or HiFormer may introduce slight bias; however, the observed performance trends remain consistent, including among larger SMAs such as MISSFormer and SU-Mamba.

Future work. To further investigate cross-domain applicability, we plan to extend this study to additional architectures and modalities, systematically assessing OOD generalization by reserving related datasets for evaluation where appropriate (e.g., Kvasir-SEG alongside NeoPolyp). Moreover, the benchmarking tool will be released as a curated, well-documented open-source resource with extended evaluation utilities to support community research and further development; the current version is already usable at GitHub.

Conclusion. Overall, our findings encourage greater awareness of resource-conscious research practices in MIS. They support the systematic evaluation of existing GP-VMs prior to introducing new task-specific architectures, thereby promoting informed model selection and efficient allocation of research resources. In scenarios where GP-VMs already achieve competitive performance, efforts may instead be directed toward other aspects of high practical relevance, including data curation, training protocol optimization, and rigorous assessment of OOD generalization behavior. Notably, these observations should be interpreted as complementary rather than contradictory to ongoing research on specialized medical architectures, whose continued development remains essential for addressing clinical scenarios in which GP-VMs may not perform adequately.

References

1. Ali, M., Wu, T., Hu, H., Luo, Q., Xu, D., Zheng, W., Jin, N., Yang, C., Yao, J.: A review of the segment anything model (sam) for medical image analysis: Accomplishments and perspectives. *Computerized Medical Imaging and Graphics* **119** (2025)
2. Borst, V., Dittus, T., Dege, T., Schmieder, A., Kounev, S.: WoundAmbit: Bridging state-of-the-art semantic segmentation and real-world wound care. In: *Machine Learning and Knowledge Discovery in Databases. Applied Data Science Track* (2025)
3. Chen, J., Wolfe, C., Kyrillidis, T.: REX: Revisiting budgeted training with an improved schedule. In: *MLSys* (2022)
4. Codella, N., Rotemberg, V., Tschandl, P., Celebi, M.E., Dusza, S., Gutman, D., Helba, B., Kalloo, A., Liopyris, K., Marchetti, M., Kittler, H., Halpern, A.: Skin lesion analysis toward melanoma detection 2018: A challenge hosted by the international skin imaging collaboration (ISIC) (2019)
5. Gotkowski, K., Gonzalez, C., Bucher, A., Mukhopadhyay, A.: M3d-CAM: A PyTorch library to generate 3D attention maps for medical deep learning. In: *Bildverarbeitung für die Medizin* (2021)
6. Gu, A., Dao, T.: Mamba: Linear-time sequence modeling with selective state spaces. In: *First conference on language modeling* (2024)
7. Guo, M.H., Lu, C.Z., Hou, Q., Liu, Z.N., Cheng, M.M., Hu, S.M.: SegNeXt: Rethinking convolutional attention design for semantic segmentation. In: *NeurIPS* (2022)
8. Heidari, M., Kazerouni, A., Soltany, M., Azad, R., Aghdam, E.K., Cohen-Adad, J., Merhof, D.: HiFormer: Hierarchical multi-scale representations using transformers for medical image segmentation. In: *WACV* (2023)
9. Huang, X., Deng, Z., Li, D., Yuan, X., Fu, Y.: MISSFormer: An effective transformer for 2D medical image segmentation. *IEEE TMI* **42** (2022)
10. Khan, W., Leem, S., See, K.B., Wong, J.K., Zhang, S., Fang, R.: A comprehensive survey of foundation models in medicine. *IEEE Reviews in Biomedical Engineering* **19** (2026)
11. Kirillov, A., Mintun, E., Ravi, N., Mao, H., Rolland, C., Gustafson, L., Xiao, T., Whitehead, S., Berg, A.C., Lo, W.Y., et al.: Segment anything. In: *ICCV* (2023)
12. Leclerc, S., Smistad, E., Pedrosa, J., Østvik, A., Cervnansky, F., Espinosa, F., Espeland, T., Berg, E.A.R., Jodoin, P.M., Grenier, T., Lartizien, C., D’hooge, J., Lovstakken, L., Bernard, O.: Deep learning for segmentation using an open large-scale dataset in 2D echocardiography. *IEEE TMI* **38** (2019)
13. Li, C., Liu, X., Li, W., Wang, C., Liu, H., Liu, Y., Chen, Z., Yuan, Y.: U-KAN makes strong backbone for medical image segmentation and generation. In: *AAAI* (2025)
14. Liu, J., Yang, H., Zhou, H.Y., Xi, Y., Yu, L., Li, C., Liang, Y., Shi, G., Yu, Y., Zhang, S., Zheng, H., Wang, S.: Swin-UMamba: Mamba-based UNet with ImageNet-based pretraining. In: *MICCAI* (2024)
15. Micikevicius, P., Narang, S., Alben, J., Diamos, G., Elsen, E., Garcia, D., Ginsburg, B., Houston, M., Kuchaiev, O., Venkatesh, G., et al.: Mixed precision training. In: *ICLR* (2018)
16. Moglia, A., Leccardi, M., Cavicchioli, M., Maccarini, A., Marcon, M., Mainardi, L., Cerveri, P.: Generalist models in medical image segmentation: A survey and performance comparison with task-specific approaches. *Information Fusion* **127** (2026)

17. Renard, F., Guedria, S., Palma, N.D., Vuillerme, N.: Variability and reproducibility in deep learning for medical image segmentation. *Scientific Reports* **10** (2020)
18. Ronneberger, O., Fischer, P., Brox, T.: U-Net: Convolutional networks for biomedical image segmentation. In: *MICCAI* (2015)
19. Sang, D.: BKAI-IGH neopolyp (2021)
20. Shi, D.: TransNeXt: Robust foveal visual perception for vision transformers. In: *CVPR* (2024)
21. Siddique, N., Paheding, S., Elkin, C.P., Devabhaktuni, V.: U-Net and its variants for medical image segmentation: A review of theory and applications. *IEEE Access* **9** (2021)
22. Tschandl, P., Rosendahl, C., Kittler, H.: The HAM10000 dataset, a large collection of multi-source dermatoscopic images of common pigmented skin lesions. *Scientific data* **5** (2018)
23. Varoquaux, G., Cheplygina, V.: Machine learning for medical imaging: methodological failures and recommendations for the future. *NPJ digital medicine* **5** (2022)
24. Wang, W., Dai, J., Chen, Z., Huang, Z., Li, Z., Zhu, X., Hu, X., Lu, T., Lu, L., Li, H., et al.: InternImage: Exploring large-scale vision foundation models with deformable convolutions. In: *CVPR* (2023)
25. Xiao, T., Liu, Y., Zhou, B., Jiang, Y., Sun, J.: Unified perceptual parsing for scene understanding. In: *ECCV* (2018)
26. Xie, E., Wang, W., Yu, Z., Anandkumar, A., Alvarez, J.M., Luo, P.: SegFormer: Simple and efficient design for semantic segmentation with transformers. In: *NeurIPS* (2021)
27. Yan, H., Wu, M., Zhang, C.: Multi-scale representations by varying window attention for semantic segmentation. In: *ICLR* (2024)
28. Zhang, Y., Shen, Z., Jiao, R.: Segment Anything Model for medical image segmentation: Current applications and future directions. *Computers in Biology and Medicine* **171** (2024)
29. Zhou, B., Zhao, H., Puig, X., Fidler, S., Barriuso, A., Torralba, A.: Scene parsing through ade20k dataset. In: *CVPR* (2017)